NEUROIMAGE **7,** 224–231 (1998)
ARTICLE NO. NI980320

Suppression of Vascular Artifacts in Functional Magnetic Resonance Images Using MR Angiograms

Petr Hluštík,*,†,‡ Douglas C. Noll,§ and Steven L. Small*,†

**Department of Neurology, University of Maryland at Baltimore, Baltimore, Maryland 21201; †Center for Neuroscience and §Department of Radiology, University of Pittsburgh, Pittsburgh, Pennsylvania 15261; and ‡Department of Neurology, Faculty of Medicine, University of Palacky, 77900 Olomouc, Czech Republic*

Received June 20, 1997

This paper describes a method for processing functional magnetic resonance images that suppresses signal changes originating from macroscopic veins visible in acquired magnetic resonance angiograms. Finger tapping experiments were performed on a 1.5-T scanner and the response was evaluated with voxel-by-voxel cross-correlation of the time course with a sinusoid at the paradigm frequency. After applying a vascular mask to suppress signal changes under macroscopic vessels, the vascular and nonvascular subpopulations of the data were compared. By visual inspection, the method was found to remove extracortical activation while preserving activation in the parenchyma. The observed higher signal amplitudes and temporal phase lags of the vascular population agree with theoretical models and previous studies. A significant portion of negatively correlated voxels occurs adjacent to through-plane vessels. Finally, comparing the centers of mass of the activated area before and after vascular suppression showed significant shifts in some subjects. © 1998 Academic Press

INTRODUCTION

Most current functional MRI (fMRI) studies use blood oxygenation level-dependent (BOLD) contrast. Several recent fMRI studies investigating the source of the MR signal change accompanying cortical activation have examined the contribution of macroscopic vessels to the BOLD signal, suggesting possible roles for blood flow, inflow effects (Duyn *et al.*, 1994), pulsatility ("vascular noise" (Ogawa *et al.*, 1993)), or pooling of oxygenated blood on the venous side of the cerebral vascular system (Lai *et al.*, 1993; Segebarth *et al.*, 1994; Lee *et al.*, 1995). Several studies (Lai *et al.*, 1993; Haacke *et al.*, 1994; Segebarth *et al.*, 1994) compared fMRI activation images with MR angiograms (MRAs) for the same slice and found a marked similarity between the significantly activated areas of the functional image and the underlying macroscopic vasculature.

Macroscopic vessels drain relatively large areas of cerebral cortex. Even the smallest pial extracortical veins (diameters of 100 to 400 μm) drain a large cortical volume by means of multiple intracortical branches. A principal intracortical vein serves a conically shaped region with an apex at the gray matter surface and a base of 1 to 4 mm in diameter at the gray/white matter junction (Duvernoy *et al.*, 1981). Concerns have been raised that the predominance of extracerebral vascular signals in fMRI data at 1.5 T may result in inaccurate localization of neural cortical activity because macrovascular signal may be located at a distance from the activated brain cortex (Segebarth *et al.*, 1994). Draining veins adjacent to a region of activated cortex may change its apparent size and center of mass. Furthermore, signals arising from vascular pulsatility may be spatially unrelated to neural activation. Finally, the dependence of activation patterns on venous vascular anatomy, which differs greatly from one person to the next, may cause difficulties in cross-subject comparisons (Segebarth *et al.*, 1994).

Biophysical models (Ogawa *et al.*, 1993; Boxerman *et al.*, 1995) show that at lower magnetic field strengths (i.e., $\leq$1.5 T), the contribution of macroscopic vessels ($>$100 μm) to fMRI signal may be more significant and harder to separate from that of microscopic intracortical vessels than at higher field strengths (Boxerman *et al.*, 1995). Thus, fMRI studies conducted on clinical MR scanners at lower field strengths have to address the issue of uncertain signal origin.

Certain pulse sequences can be used to suppress macrovascular signals during MR data acquisition, such as spin echo rather than gradient echo (Bandettini *et al.*, 1994) or to minimize inflow with long TR, small flip angles (Boecker *et al.*, 1994; Frahm *et al.*, 1994), volume acquisitions (Haacke *et al.*, 1994), or spatial presaturation (Duyn *et al.*, 1994). Glover *et al.* (1996) designed a dual-echo spiral gradient-recalled echo pulse sequence to separate BOLD effects from inflow effects.

1053-8119/98 $25.00

Alternatively, the macrovascular voxel population can be removed by postprocessing. Several intrinsic signal properties can be used to decide whether or not a signal from a particular voxel is of macrovascular origin: (1) The signal deviation from baseline should be proportional to fractional blood volume in the voxel and therefore the size of the vessel (Ogawa *et al.*, 1993); (2) when extrapolating from 4 to 1.5 T with echo times relatively short compared to T_2^*, activated gray matter should yield 1–2% signal change while 5% or greater changes likely correspond to regions of large venous blood vessel or arise as a result of inflow (Menon *et al.*, 1993); (3) when determining the temporal phase delays that give the maximal cross-correlation between the signal time course and a sinusoidal model curve (Bandettini *et al.*, 1993), signals that correspond anatomically to macroscopic blood vessels should be the most delayed, have a high correlation magnitude, and have a high peak-to-peak signal deviation from baseline (Lee *et al.*, 1995). Other parameters found to correlate with the presence of a large vein are positive slope of a "trend" line through the time course and a high value of the ratio of NMR phase over NMR magnitude (Lee *et al.*, 1995). Selected signal properties can be used to separate macroscopic vessels from parenchyma by multidimensional clustering techniques (Gaser *et al.*, 1996; Singh *et al.*, 1996).

In this study, we used magnetic resonance angiograms in an alternative approach that is independent of voxel size, task design, or timing pattern and does not lead to a loss of fMRI sensitivity. To develop and test the method, we used a motor task to activate a distributed brain system that is well described (see Donoghue and Sanes, 1994, for review of cortical motor areas) and for which the corresponding fMRI activation is known (Rao *et al.*, 1993). We acquired MRAs in the same planes as the functional images and used them to suppress vascular signals. In addition to visual evaluation of the results, peak-to-peak signal deviation from baseline and temporal phase delays were studied separately for the vascular and nonvascular voxels. Center of mass analysis was performed to investigate the influence of vascular suppression on the location of activation within a region of interest.

METHODS

Subjects and Task

Five normal subjects (four right-handed, one left-handed) performed sequential opposition of fingers to thumb at 2 Hz alternating with a rest control, each phase lasting 24 s. Four complete cycles (repetitions of each condition pair) were performed. Each subject performed three repetitions of the task and the data were averaged within subject to increase statistical power.

Imaging and Data Analysis

Subjects were imaged using a 1.5-T clinical scanner (General Electric Medical Systems Signa). Bilateral 5-in. surface coils were positioned above the ears and nine axial slices were prescribed from the vertex down. Anatomical images were T1-weighted (spin echo, TR = 500 ms, TE = 16 ms). MRAs were acquired as 2D phase contrast angiography (gradient echo, flip angle = 25°, TE = 6 ms, TR = 25 ms, 192 × 256 matrix, velocity encoding 10 cm/s in all directions). Slice locations of the MRAs exactly matched the anatomical and functional scans. The pulse sequence and velocity encoding were chosen to be specific to veins and venules and to maximize the visualization of slow flow. To justify the velocity encoding, we observed the transit of contrast agent through cortical draining veins during catheter angiography, which corresponded to flow velocity about 2–4 cm/s.

Functional images (T2*-weighted) were acquired using spiral gradient echo imaging (200 mm field of view, four spirals, nine slices 4 mm thick, 3.1 mm in-plane resolution, TR = 750 ms, flip angle = 40°, TE = 35 ms, nine slices acquired every 3 s, 64 repeats, total image acquisition time 189 s). The specific spiral design has been described in detail elsewhere (Noll *et al.*, 1995). Correction for magnetic field nonuniformity (Noll *et al.*, 1991) was used to insure accurate overlay of angiograms to fMRI maps. Reconstructed images were movement corrected using Automated Image Registration software (AIR, Woods *et al.*, 1993) and a 2D rigid model.

Data were analyzed using cross-correlation with a sinusoidal model curve (Bandettini *et al.*, 1993). Correlation with sine and cosine reference waveforms (Lee *et al.*, 1995) was used to find the maximum correlation coefficient and the corresponding temporal phase lag. Fourier analysis of signal time course was performed for each voxel and the spectral magnitude at the paradigm frequency was used to estimate the signal change (Lee *et al.*, 1995), while the zero frequency spectral component was used to estimate the baseline. The peak-to-peak percent signal deviation from baseline was then calculated as twice the ratio of spectral magnitude at the paradigm frequency to the zero frequency component. We used correlation threshold of $r = 0.5$ and a three-dimensional contiguity threshold (Forman *et al.*, 1995) to generate the raw statistical images.

Angiogram Processing and Masking

The set of contiguous MRAs was smoothed with a 3D gaussian filter of 4 mm full width at half-maximum in all three dimensions to account for the lower resolution

of the functional image, vascular signal field effects extending beyond vessel borders, and possible displacement of oblique vessels due to differences in echo time. The resulting blurred MR angiographic images were thresholded using an intensity threshold and a 3D contiguity threshold (Forman *et al.*, 1995). The intensity threshold was set to the image mean plus two standard deviations. The acquired vascular mask (up to 6 mm wide for major cortical veins) was then used to suppress the overlying voxels in the statistical image. The remaining (presumably nonvascular) voxel population was thresholded using the same correlation coefficient and 3D contiguity as the raw images to get the processed statistical image.

Evaluation

Three methods were used to evaluate the success of vascular artifact suppression: First, the original and processed functional images were viewed and compared by two independent observers. True activation included (1) activation limited to cortical gray matter and (2) location of each activated region in agreement with available evidence from physiological and previous functional imaging studies of hand movement (Rao *et al.*, 1993). Second, the populations of vascular and nonvascular voxels in the statistical image were compared with respect to their peak-to-peak signal deviations as a percentage of baseline. Third, the vascular and nonvascular voxels were compared regarding the temporal phase delays associated with maximal size of the correlation coefficient. Basic statistical parameters and histograms of signal deviations and temporal phase lags were calculated for voxels with $r > 0.35$ in each slice. This relatively low threshold was used to show the considerable population of voxels with negative phase (180° to 360°) that diminished at higher correlation thresholds.

A center of mass analysis before and after vascular artifact suppression was performed on a large rectangular region of interest comprising the lateral and middle (in the anterior–posterior direction) ninth of the imaged cortex and containing the primary sensorimotor cortices contralateral to the moving hand.

RESULTS

Subjective Evaluation

The "raw" statistical images contained activation in the primary motor (M1) and sensory cortices (pre- and postcentral gyri, Brodmann areas 4 and 1–3), lateral premotor cortex (area 6 on the convexity), and supplementary motor area (SMA, mesial area 6). In addition, there were occasional activation foci in the subdural space and sulci. The "processed" statistical images show a substantial reduction of the extracortical activated areas, while activation in the gray matter was preserved. Figure 1 shows one axial slice at the level of the contralateral (right) M1 hand area activated with left finger movement. Further activated foci were ipsilateral (left) M1 and SMA. Overlap of activation and blurred vessels can be seen at the outer edge of the right M1 and the anterior edge of SMA.

All subjects showed similar activation in the middle genu of the precentral gyrus, corresponding to the primary motor hand area (Yousry *et al.*, 1997). The additional activation patterns as well as the venous vascular patterns showed greater variability. The image and histogram data shown below were derived from a single subject (subject 1) for the sake of consistency.

Vascular versus Nonvascular Voxel Signal Analysis

Mean and median values of temporal phase delays and signal deviations from baseline for the suppressed (vascular) and remaining (nonvascular) voxels for all five subjects are shown in Table 1. Vascular voxels have consistently higher mean and median signal deviations from baseline in all slices. Superiorly toward the vertex, the mean and median signal amplitudes increase primarily for the vascular voxels. Mean temporal delays were calculated for the interval between 0 and 16 s (0 to 120°) that contains most of the activation. Average delays across five subjects were about the same for the vascular and nonvascular voxels in the lower slices; in the top slices 1 and 2, vascular voxels are delayed on average by 0.4 and 0.3 s, respectively, after nonvascular voxels.

The results of a more detailed analysis are shown for one slice in subject 1 (slice 6, the same as in Fig. 1). The histograms of signal deviation from baseline show overlapping but distinct peaks for the vascular and nonvascular voxels (Fig. 2). The histogram of temporal phase lags has two peaks for the nonvascular voxels, early and late, about 180° (24 s) apart, and one early peak for the vascular voxels (Fig. 3). Plots of peak-to-peak signal deviation from baseline versus temporal phase show a single early peak for the vascular voxels at about 6 s (Fig. 4), coincidental with the early peak of the temporal phase histograms in Fig. 3. The nonvascular population shows also a strong early peak and more voxels at later phases (Fig. 5). Comparison of Figs. 3 and 5 shows that the late peak in the phase histogram consists mostly of voxels with low signal amplitude (around 1%).

A center of mass analysis showed that the effect of vascular suppression on the centroid of activation is small, producing individually variable shifts on the order of single millimeters (Table 2). The most consistent change is a center of mass shift toward the midline and away from the surface of the brain.

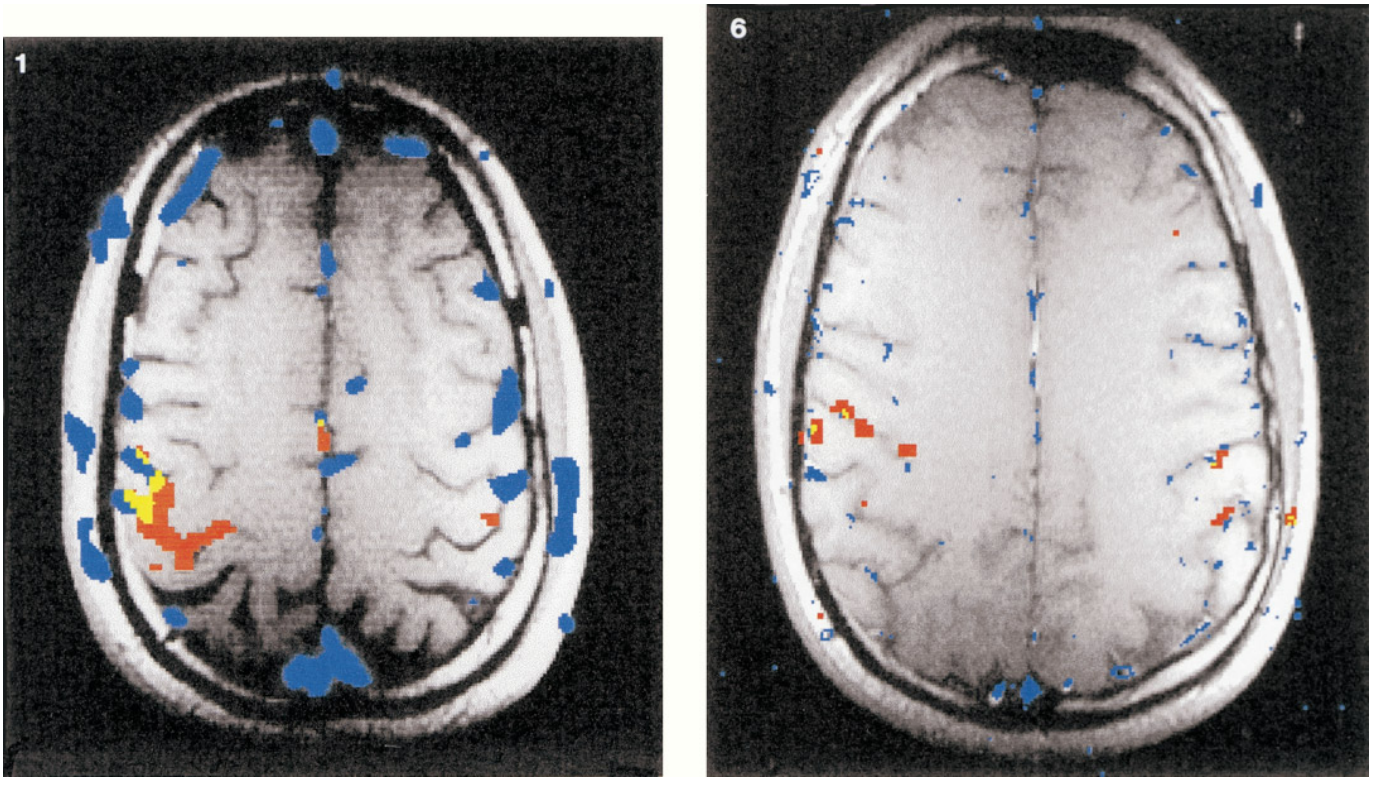

FIG. 1. Axial slice through the primary motor cortical hand area activated with left (dominant) finger movement. Overlay image showing fMRI activation (red), blurred angiogram (blue), and their overlap (yellow) over an anatomical MR image. Correlation image is thresholded at $r = 0.5$. Left side of the brain is on the right.

FIG. 6. Overlay image showing out-of-phase fMRI activation (red), venous MR angiogram (blue), and their overlap (yellow) over an anatomical MR image for an axial slice through the primary motor cortex. Correlation image is thresholded at $r = 0.5$.

Analysis of significantly activated foci with negative phase indicated their location to be within 2–5 mm of through-plane macroscopic veins adjacent to motor cortical areas and mostly on the activated (contralateral) side of the brain (Fig. 6). In some cases, there were no MRA-visible vessels nearby but the negative phase region was found to adjacent to a significantly activated area with a positive phase. The temporal delay of the negative foci was typically in the range of 190° to 260° (25 to 35 s in the 48-s cycle).

TABLE 1

Means and Standard Deviations (in Parentheses) of Signal Properties for the Vascular (v) and Nonvascular (nv) Voxels[a] Across Subjects

			Signal deviation from baseline (%)							
	Voxel count		Mean		Median		Maximum		Delay[b]	
Slice	v	nv	v	nv	v	nv	v	nv	v	nv
1	539 (349)	2335 (1590)	5.0 (1.8)	2.5 (0.5)	4.0 (1.2)	1.9 (0.4)	19.3 (9.2)	14.6 (9.8)	7.3 (2.1)	6.9 (1.1)
2	454 (350)	2575 (1905)	4.4 (1.8)	1.9 (0.4)	3.9 (1.4)	1.4 (0.3)	13.6 (11.1)	11.2 (6.4)	7.1 (2.1)	6.8 (1.1)
3	375 (296)	3407 (2324)	3.2 (0.8)	1.8 (0.3)	2.6 (0.8)	1.3 (0.2)	10.7 (4.2)	10.6 (0.9)	7.0 (2.2)	7.1 (0.9)
4	443 (356)	3956 (2359)	3.4 (1.2)	1.5 (0.1)	2.9 (1.1)	1.2 (0.1)	9.0 (3.2)	8.0 (1.9)	6.9 (2.2)	6.9 (0.6)
5	449 (346)	4108 (2069)	3.0 (0.8)	1.5 (0.2)	2.3 (0.3)	1.1 (0.1)	10.3 (5.7)	8.9 (3.0)	7.0 (2.0)	6.9 (0.4)
6	410 (279)	4138 (1861)	2.2 (0.2)	1.4 (0.2)	1.9 (0.3)	1.1 (0.2)	7.1 (1.3)	7.9 (1.0)	6.9 (1.9)	6.8 (0.5)
7	433 (369)	4571 (1902)	2.4 (1.5)	1.4 (0.2)	2.1 (1.2)	1.1 (0.1)	8.9 (6.8)	10.5 (4.1)	6.7 (1.9)	6.7 (0.5)
8	557 (434)	4330 (2316)	2.3 (1.0)	1.3 (0.1)	1.9 (0.8)	1.1 (0.1)	7.7 (3.2)	7.4 (2.0)	6.5 (1.9)	6.5 (0.5)
9	509 (379)	4030 (1675)	1.8 (0.7)	1.2 (0.2)	1.4 (0.6)	1.0 (0.1)	7.6 (3.8)	7.6 (3.1)	6.4 (1.9)	6.6 (0.5)
All	463 (345)	3717 (1944)	3.1 (0.5)	1.6 (0.2)	2.6 (0.5)	1.2 (0.2)	10.5 (2.9)	9.6 (2.7)	6.9 (2.0)	6.8 (0.5)

[a] Only voxels with correlation coefficient >0.35 are included.
[b] Temporal phase delays are averaged across the initial 16 s (120°).

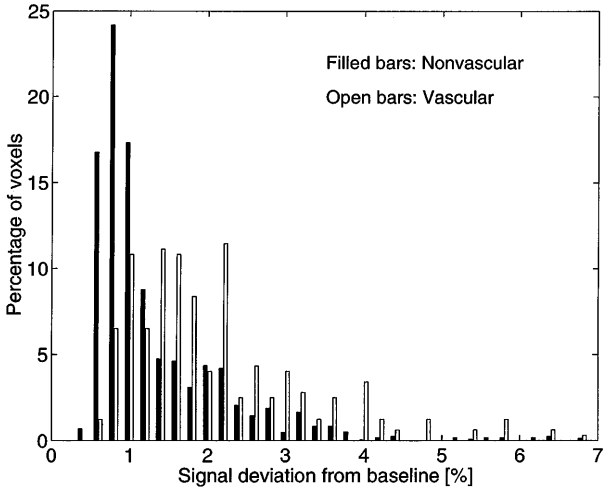

FIG. 2. Histograms of peak-to-peak signal deviation (percentage of baseline) for the vascular and nonvascular voxels in the axial slice from Fig. 1. Only voxels with correlation >0.35 are shown.

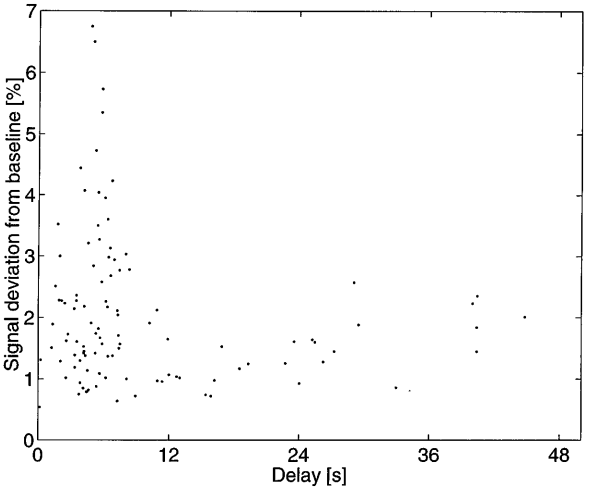

FIG. 4. Distribution of peak-to-peak signal deviation (percentage of baseline) along the temporal phase for vascular voxels with correlation >0.35 (same slice as Fig. 1).

DISCUSSION

This study was motivated by the fact that no current strategy to eliminate macrovascular contribution to the fMRI signal provides a complete and practical solution. The functional imaging pulse sequence employed in this study contained a combination of long TR (750 ms) with a modest flip angle (40°) to reduce sensitivity to inflow, yet a significant fraction of the activation appeared vascular in origin. This finding seems to justify the use of postprocessing in addition to strategies reducing inflow.

The present method yielded satisfactory results with visual evaluation. Satisfying our criteria, the nonvascular voxels were mainly located in gray matter in the cortical areas involved in hand movement generation and control, as expected for the finger tapping task (Rao *et al.*, 1993). Even though the vascular mask occasionally overlapped the edge of gray matter, the intracortical activation was mostly unaffected by masking.

Higher mean and median signal deviation of the rejected voxels support the expectation of their macrovascular origin. Higher signal deviations in slices closer to the vertex are consistent with pooling of oxygenated blood in draining veins (Lai *et al.*, 1993; Segebarth *et al.*, 1994; Lee *et al.*, 1995). Furthermore, a voxel located across these large vessels is likely to contain a high fraction of blood and lower partial volume effect. In each subject, voxels with very large signal deviation (up to 32%) belonged to the vascular population.

The temporal character of the response in the vascular voxel population is quite simple with a single strong

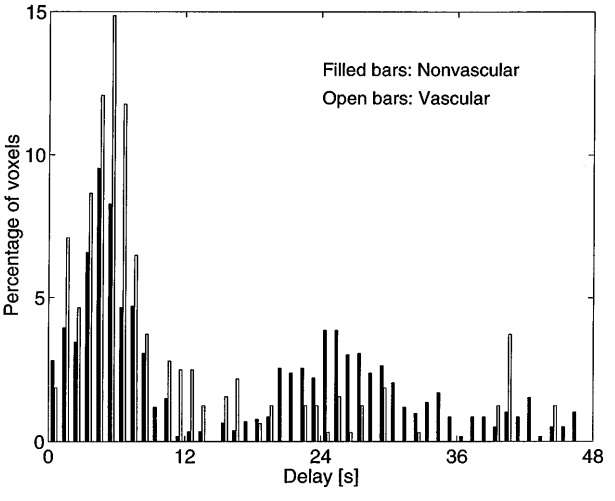

FIG. 3. Histograms of temporal phase delays for the vascular voxels and nonvascular voxels with correlation >0.35 (same slice as Fig. 1).

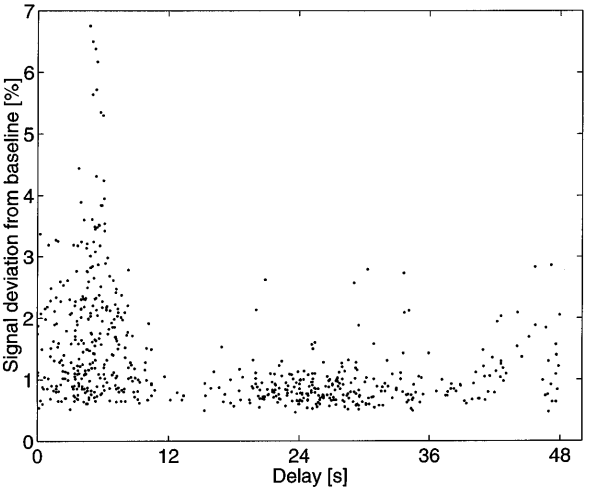

FIG. 5. Distribution of peak-to-peak signal deviation (percentage of baseline) along the temporal phase for nonvascular voxels with correlation >0.35 (same slice as Fig. 1).

TABLE 2

Center of Mass Shifts for Primary Sensorimotor Cortical Regions (in Millimeters)

Subject	Medial–lateral	Anterior–posterior	Inferior–superior	Distance
1	0.7	1.7	1.4	2.3
2	1.0	−0.9	−0.4	1.4
3	1.2	1.1	0.2	1.6
4	0.1	0.1	0.2	0.2
5	0.9	0.1	0	0.9
Mean	0.8	0.4	0.3	1.3
SD	0.4	1.0	0.7	0.8

Note. Positive sign means shift medially, posteriorly, and inferiorly; distance represents a square root of the sums of squares of the shifts along the three axes.

early peak at about 6 s composed of a relatively high number of voxels (as shown in the histogram in Fig. 3) with high signal amplitude (see Fig. 4). The nonvascular voxel population shows a more complicated behavior. The temporal phase is clearly bimodal, in agreement with the observation of Saad *et al.* (1996). The second peak of the temporal phase delay histogram (Fig. 3) contains most of the negatively correlated voxels. These voxels are not located directly over vessels and are not identified as vascular by our method. However, most of them seem to be located adjacent to an MRA visible through-plane vessel (Fig. 6). Negative correlation with a sinewave can be either a product of a "negative" signal (decrease during the active task relative to rest) or a "positive" signal (signal higher during the active task) delayed by half-cycle. The latter alternative seems to be ruled out by the fact that voxels 180° out of phase are consistently observed with paradigms of different cycle duration (Lee *et al.*, 1995; Saad *et al.*, 1995, 1996).

The phase delays of the negative foci suggest that their signal changes could be related to signals from vessels or parenchyma whose responses peak a half-cycle (180°) earlier.

Negatively correlated voxels were observed previously in fMRI (Kim *et al.*, 1992; Listerud *et al.*, 1994; Lalonde *et al.*, 1995, 1996; Lee *et al.*, 1995; van Gelderen *et al.*, 1995; Popp *et al.*, 1996; Yamamoto *et al.*, 1996). In our study, the close spatial relation of negatively correlated voxels to vessels agrees with the findings of Popp *et al.* (1996). The negative foci could arise from venous blood susceptibility-based frequency shifts (Jesmanowicz *et al.*, 1994). In spiral scanning, such a frequency shift would not cause a direct spatial shift in the phase encoding direction as expected in echo-planar imaging (Jesmanowicz *et al.*, 1994) but rather a degradation of the point spread function. Frequency shifts in veins reported by Lai *et al.* (1995, 1996) could be enough to induce negative side lobes in the point spread function for spiral imaging (Noll *et al.*, 1991). The signal changes in a voxel adjacent to a draining vein could then have an opposite direction. Some physiological causes for negatively correlated signals related to vessels include flow effects, signals from vessels draining an activated area where the increase in neuronal activity and metabolism has not been compensated by excess oxygen delivery, or a rather improbable steal phenomenon that has been reported only under pathological brain conditions (Tarr *et al.*, 1990). Negatively correlated response might also be independent of vessels, originating from areas where neuronal activation actually decreases during the task relative to rest. This would correspond to a finding that negative correlations in fMRI are colocalized with regional cerebral blood flow decreases in PET (Lalonde *et al.*, 1995). The amplitude of the oscillatory response is quite small in the counterphase voxels (see Fig. 5), so at least some of them may represent noise. Further work with higher resolution functional images and angiograms may be necessary to explain the origin of the negative-phase voxels.

While the center of mass shifts after vascular suppression were smaller than the in-plane resolution, there was a consistent medial shift, away from the veins on the lateral brain surface. Considering that the large draining veins are located in the most superior slices, we would also expect a more significant shift inferiorly with vascular suppression. On the other hand, most of the BOLD effect may have diluted before reaching the top slices. The observed variability of center of mass changes could be attributed to the individual patterns of draining veins. In subject 1, a conspicuous vein draining the central sulcus continues anteriorly and upwards and this course could explain the extension of the unprocessed primary sensorimotor cortical activation in the same direction. Most of our subjects did not show any consistent and significant shifts after vascular suppression, which could correspond to the observation of insignificant differences between PET and fMRI motor activation by Ramsey *et al.* (1996). Because of the described variability, this issue deserves consideration by fMRI studies aiming at assessing exact location and/or extent of the activated regions.

There are several limitations of the presented method: (a) angiogram processing by blurring and thresholding can remove small weak vessels and their effects may not be accounted for; (b) choosing a particular value of velocity encoding for the MRA acquisition results in suboptimal encoding of much slower or faster flow; and (c) widening the vessels to match the in-plane resolution may not be enough to cover displaced signals from vessels flowing obliquely through the slice plane. Table 1 and the signal amplitude histogram (Fig. 2) show that the nonvascular population contains some voxels with very large changes (up to 13% for four of

five subjects, up to 32% for subject 2). These are usually located outside of the brain not far away from vessels with even higher signals, but the finding may support the idea that perfect elimination of vascular signals was still not achieved.

In summary, although the described method is limited by the spatial resolution of the MRAs, it is applicable to any fMRI study complemented with MRA acquisition. The method reduces the number and extent of "false" activated regions without reducing fMRI sensitivity. In this way, it can contribute to more precise localization of activation and may therefore be useful as an additional image processing step in fMR image analysis.

ACKNOWLEDGMENTS

Support of NIH Grants NINDS NS32756 to the second author, R01-NS37195 and R01-CD3378 to the last author, and the MR Research Center of the University of Pittsburgh Medical Center is gratefully appreciated. Special thanks to Rao Gullapalli for informative discussions, to Mark Hahn and Darren Emge for helping with software development, and to the subjects.

REFERENCES

Bandettini, P. A., Jesmanowicz, A., Wong, E. C., and Hyde, J. S. 1993. Processing strategies for time-course data sets in functional MRI of the human brain. *Magn. Reson. Med.* **30:**161–173.

Bandettini, P. A., Wong, E. C., Jesmanowicz, A., Hinks, R. S., and Hyde, J. S. 1994. Spin-echo and gradient-echo EPI of human brain activation using BOLD contrast: A comparative study at 1.5 T. *NMR Biomed.* **7:**12–20.

Boecker, H., Kleinschmidt, A., Requardt, M., Hanicke, W., Merboldt, K. D., and Frahm, J. 1994. Functional cooperativity of human cortical motor areas during self-paced simple finger movements: A high-resolution MRI study. *Brain* **117:**1231–1239.

Boxerman, J. L., Bandettini, P. A., Kwong, K. K., Baker, J. R., Davis, T. L., Rosen, B. R., and Weisskoff, R. M. 1995. The intravascular contribution to fMRI signal change: Monte Carlo modeling and diffusion-weighted studies in vivo. *Magn. Reson. Med.* **34:**4–10.

Donoghue, J. P., and Sanes, J. N. 1994. Motor areas of the cerebral cortex. *J. Clin. Neurophysiol.* **11:**382–396. [Review]

Duvernoy, H. M., Delon, S., and Vannson, J. L. 1981. Cortical blood vessels of the human brain. *Brain Res. Bull.* **7:**519–579.

Duyn, J. H., Moonen, C. T., van Yperen, G. H., de Boer, R. W., and Luyten, P. R. 1994. Inflow versus deoxyhemoglobin effects in BOLD functional MRI using gradient echoes at 1.5 T. *NMR Biomed.* **7:**83–88.

Forman, S. D., Cohen, J. D., Fitzgerald, M., Eddy, W. F., Mintun, M. A., and Noll, D. C. 1995. Improved assessment of significant activation in functional magnetic resonance imaging (fMRI): Use of a cluster-size threshold. *Magn. Reson. Med.* **33:**636–647.

Frahm, J., Merboldt, K. D., Hanicke, W., Kleinschmidt, A., and Boecker, H. 1994. Brain or vein—oxygenation or flow? On signal physiology in functional MRI of human brain activation. *NMR Biomed.* **7:**45–53.

Gaser, C., Volz, H.-P., Haeger, F., Rzanny, R., Mentzel, H.-J., Kaiser, W. A., and Sauer, H. 1996. Artifact reduction in analysis of functional MRI data using 2-dimensional histograms. In *Proceedings, ISMRM 4th Scientific Meeting, New York,* p. 1815.

Glover, G., Lemieux, S., Drangova, M., and Pauly, J. 1996. Decomposition of inflow and blood oxygen level-dependent (BOLD) effects with dual-echo spiral gradient-recalled echo (GRE) fMRI. *Magn. Reson. Med.* **35:**299–308.

Haacke, E. M., Hopkins, A., Lai, S., Buckley, P., Friedman, L., Meltzer, H., Hedera, P., Friedland, R., Klein, S., and Thompson, L. 1994. 2D and 3D high resolution gradient echo functional imaging of the brain: venous contributions to signal in motor cortex studies. *NMR Biomed.* **7:**54–62.

Jesmanowicz, A., Bandettini, P., and Hyde, J. 1994. Frequency shift artifacts in functional echo-planar imaging. In *Proceedings, SMR 2nd Scientific Meeting, San Francisco,* p. 437.

Kim, S. G., Merkle, H., Ashe, J., Georgopoulos, A. P., Menon, R. S., Ellermann, J. M., Ogawa, S., Tank, D. W., and Ugurbil, K. 1992. Functional mapping of human motor cortex at high magnetic field. In *Proceedings, SMRM 11th Annual Meeting, Berlin,* p. 1825.

Lai, S., Haacke, E., Lin, W., Chien, D., and Levin, D. 1995. *In vivo* measurement of cerebral venous blood oxygenation with MRI. In *Proceedings, SMR 3rd Scientific Meeting, Nice, France,* p. 849.

Lai, S., Haacke, E. M., Reichenbach, J., Kuppusamy, K., Hoogenraad, F., Takeichi, H., and Lin, W. 1996. *In vivo* quantification of brain activation-induced change in cerebral blood oxygen saturation using MRI. In *Proceedings, ISMRM 4th Scientific Meeting, New York,* p. 1756.

Lai, S., Hopkins, A. L., Haacke, E. M., Li, D., Wasserman, B. A., Buckley, P., Friedman, L., Meltzer, H., Hedera, P., and Friedland, R. 1993. Identification of vascular structures as a major source of signal contrast in high resolution 2D and 3D functional activation imaging of the motor cortex at 1.5T: Preliminary results. *Magn. Reson. Med.* **30:**387–392.

Lalonde, F. M., Jezzard, P., Weisberg, J. A., Wiggs, C. L., Haxby, J. V., and Martin, A. 1996. A difference in fMRI time courses between areas of increased and decreased neural activity. *NeuroImage* **3:**S74.

Lalonde, F. M., Martin, A., Weisberg, J. A., Maisog, J. M., and Haxby, J. V. 1995. Identification of areas of increased and decreased neural activity using fMRI. *Human Brain Mapping* **1:**S230.

Lee, A. T., Glover, G. H., and Meyer, C. H. 1995. Discrimination of large venous vessels in time-course spiral blood-oxygen-level-dependent magnetic-resonance functional neuroimaging. *Magn. Reson. Med.* **33:**745–754.

Listerud, J., Lopez-Villegas, L., Isaac, G., Atlas, S., Detre, J., and Alsop, D. 1994. Validation of regions of positive and negative correlation to stimulus observed on Student's t maps calculated from functional MRI studies in normal volunteers. In *Proceedings, SMR 2nd Annual Meeting, San Francisco,* p. 634.

Menon, R. S., Ogawa, S., Tank, D. W., and Ugurbil, K. 1993. 4 Tesla gradient recalled echo characteristics of photic stimulation-induced signal changes in the human primary visual cortex. *Magn. Reson. Med.* **30:**380–386.

Noll, D. C., Cohen, J. D., Meyer, C. H., and Schneider, W. 1995. Spiral K-space MR imaging of cortical activation. *J. Magn. Reson. Imaging* **5:**49–56.

Noll, D. C., Meyer, C. H., Pauly, J. M., Nishimura, D. G., and Macovski, A. 1991. A homogeneity correction method for magnetic resonance imaging with time-varying gradients. *IEEE Trans. Med. Imag.* **10:**629–637.

Ogawa, S., Menon, R. S., Tank, D. W., Kim, S. G., Merkle, H., Ellermann, J. M., and Ugurbil, K. 1993. Functional brain mapping by blood oxygenation level-dependent contrast magnetic resonance imaging: A comparison of signal characteristics with a biophysical model. *Biophys. J.* **64:**803–812.

Popp, C. A., Trudeau, J. D., Biswal, B., and Faber, T. L. 1996. Negative pixels in functional maps of sensorimotor tasks. *NeuroImage* **3:**S165.

Ramsey, N. F., Kirkby, B. S., van Gelderen, P., Berman, K. F., Duyn, J. H., Frank, J. A., Mattay, V. S., Van, H. J. D., Esposito, G., Moonen, C. T., and Weinberger, D. R. 1996. Functional mapping of human sensorimotor cortex with 3D BOLD fMRI correlates highly with H2(15)O PET rCBF. *J. Cereb. Blood Flow Metab.* **16:**755–764.

Rao, S. M., Binder, J. R., Bandettini, P. A., Hammeke, T. A., Yetkin, F. Z., Jesmanowicz, A., Lisk, L. M., Morris, G. L., Mueller, W. M., Estkowski, L. D., *et al.* 1993. Functional magnetic resonance imaging of complex human movements. *Neurology* **43:**2311–2318.

Saad, Z. S., Carman, G. J., and DeYoe, E. A. 1995. Temporal variation of FMR signals. In *Proceedings, SMR 3rd Scientific Meeting, Nice, France,* p. 813.

Saad, Z. S., Ropella, K. M., Carman, G. J., and DeYoe, E. A. 1996. Temporal phase variation of FMR signals in vasculature versus parenchyma. In *Proceedings, ISMRM 4th Scientific Meeting, New York,* p. 1834.

Segebarth, C., Belle, V., Delon, C., Massarelli, R., Decety, J., Le, B. J. F., Decorps, M., and Benabid, A. L. 1994. Functional MRI of the human brain: Predominance of signals from extracerebral veins. *NeuroReport* **5:**813–816.

Singh, M., Patel, P., and Khosla, F. 1996. Automated segmentation of fMRI using pixel-based features. In *Proceedings, ISMRM 4th Scientific Meeting, New York,* p. 1777.

Tarr, R. W., Johnson, D. W., Rutigliano, M., Hecht, S. T., Pentheny, S., Jungreis, C. A., Horton, J. A., and Yonas, H. 1990. Use of acetazolamide-challenge xenon CT in the assessment of cerebral blood flow dynamics in patients with arteriovenous malformations. *Am. J. Neuroradiol.* **11:**441–448.

van Gelderen, P., Ramsey, N. F., Liu, G., Duyn, J. H., Frank, J. A., Weinberger, D. R., and Moonen, C. T. 1995. Three-dimensional functional magnetic resonance imaging of human brain on a clinical 1.5-T scanner. *Proc. Natl. Acad. Sci. USA* **92:**6906–6910.

Woods, R. P., Mazziotta, J. C., and Cherry, S. R. 1993. MRI-PET registration with automated algorithm. *J. Comput. Assist. Tomogr.* **17:**536–546.

Yamamoto, T., Kida, I., Kajiyama, M., Tamura, M., and Miyasaka, K. 1996. Positive-negative complementary signal changes of finger tapping fMRI. In *Proceedings, ISMRM 4th Scientific Meeting, New York,* p. 1861.

Yousry, T. A., Schmid, U. D., Alkadhi, H., Schmidt, D., Peraud, A., Buettner, A., and Winkler, P. 1997. Localization of the motor hand area to a knob on the precentral gyrus: A new landmark. *Brain* **120:**141–157.